Multiferroic phases of the frustrated quantum spin chain compound linarite

K. Yu. Povarov,[1,*] Y. Feng,[1] and A. Zheludev[1]

[1] *Neutron Scattering and Magnetism, Laboratory for Solid State Physics, ETH Zürich, Switzerland*[†]

The dielectric properties of the prototypical frustrated ferromagnetic spin chain compound $PbCuSO_4(OH)_2$ known as linarite, are studied across its strongly anisotropic magnetic phase diagram on single crystal samples. The ferroelectric character of the principal low-field spin spiral phase is confirmed. The measured polarization is fully consistent with the previously proposed magnetic structure. Spontaneous polarization is also detected in two other field-induced phases, but in some cases is incompatible with previously suggested models for the spin arrangement.

arXiv:1609.06087v1 [cond-mat.str-el] 20 Sep 2016

I. INTRODUCTION

The improper ferroelectric nature of magnetically ordered phases in certain antiferromagnetic materials endows them with a rich phenomenology and potential technological applications. In recent years it has given rise to the entirely new research area of *magnetic multiferroics* [1–3]. Correlations between magnetic ordering and dielectric properties have been found in a very different classes of materials. On one end of the spectrum are rare earth compounds with a large spin value and truly dramatic magnetoelectric effects [4, 5]. The other limit are $S = 1/2$ organometallic cuprates where extreme quantum fluctuations fully suppress long-range order, which is only restored by a field-induced quantum phase transition [6, 7]. A more conventional type of multiferroic cuprates are systems featuring edge-sharing copper-oxygen chains. Among these are $LiCu_2O_2$ [8] and $LiCuVO_4$ [9], which have long served as prototype materials for the study of multiferroicity [10, 11]. In these systems the source of electric polarization is a helimagnetic arrangement of spins that breaks inversion symmetry [12, 13]. Helimagnetism, in turn, results from a geometric frustration of magnetic interactions. Specifically, the Heisenberg exchange constant J_1 between the nearest-neighbor Cu^{2+} spins is ferromagnetic, and competes with the antiferromagnetic next-nearest neighbor coupling J_2.

The most recently studied member of the frustrated copper oxide chains family is the natural mineral linarite $PbCuSO_4(OH)_2$ [14]. It is also perhaps the most interesting one: the estimated ratio of exchange constants $J_1/J_2 \simeq -2.8$ places linarite very close to the quantum critical point at $J_1/J_2 \simeq -4$, where the ferromagnetic interaction takes over and the ground state changes to a fully polarized one. At the same time, the saturation field in linarite is below 10 T, making its entire magnetic phase diagram easily accessible experimentally [15]. To date, up to five distinct magnetic phases have been identified. This complex behavior emphasizes the highly frustrated nature of this spin system and the importance of quantum spin fluctuation [15, 16]. The primary Phase I occurring at zero applied magnetic field has been identified as a spin spiral. It would be natural to expect this phase to generate non-zero electric polarization, simply by analogy to $LiCu_2O_2$ and $LiCuVO_4$. Indeed, previous studies have detected the presence of bias-induced electric polarization in linarite *powder* samples below T_N [17]. The challenge, remains to perform more detailed studies on a *single crystal* sample, in order to determine the direction of polarization, its relation to the underlying magnetic order, and its evolution in external magnetic fields. This is the issue addressed by the present study.

Blue transparent crystals of linarite belong to a monoclinic $P2_1/m$ (#11) space group. The unit cell dimensions are $a = 9.68$, $b = 5.65$, $c = 4.68$ Å, with the angle between the a and c being $\beta = 102.6°$ [18]. The structure of the material is shown in Fig. 1. There are two copper atoms per unit cell. Together with surrounding oxygen ions they form a ribbon chain of Cu-O plaquettes, propagating along the high symmetry **b** direction. Magnetization measurements supported by first-principle calculations lead to the estimate of the main exchange parameters as $J_1 \simeq -8.6$ and $J_2 \simeq 3.1$ meV [19]. A rich magnetic phase diagram (Fig. 2) was revealed below $T_N \simeq 2.8$ K [15, 16]. Five distinct magnetic phases exist for $\mathbf{H} \parallel \mathbf{b}$. The zero-field elliptic spin spiral (I) changes to a canted commensurate structure (IV) around 3 T, with the transition line splitting into regions of phase coexistence at low and high temperatures. The high-temperature region, labeled as III, is supposed to be a mixture of Phase IV and alternative spiral configuration, different from Phase I. The low-temperature II region is the metastable mixture of Phases I and IV. Finally, for $\mathbf{H} \parallel \mathbf{b}$, there is an unusual high-field phase believed to be a spin density wave state (V). Remarkably, for a magnetic field applied transverse to **b** direction, there appears to be only a single magnetic phase, namely the spiral state I.

II. EXPERIMENTAL DETAILS

The present study employed natural single crystals of linarite from the Grand Reef Mine, Arizona, USA. For all samples, the crystal structure verified at room temperature by means of X-ray diffraction (BRUKER APEX II single crystal diffractometer), and found to be in good agreement with the previously published data [15, 20].

* povarovk@phys.ethz.ch
† http://www.neutron.ethz.ch/

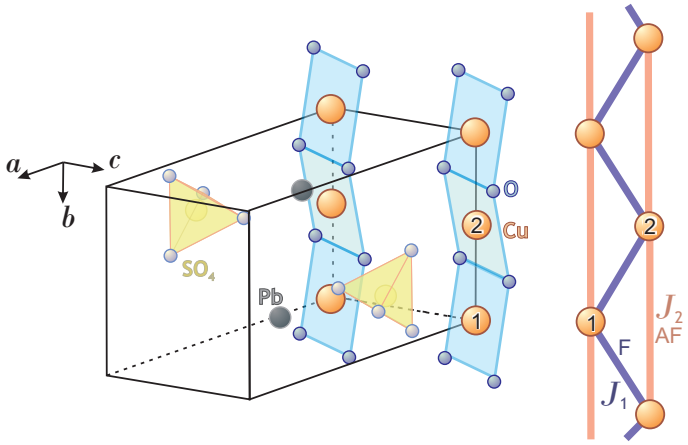

FIG. 1. Left: Crystal structure of linarite $PbCuSO_4(OH)_2$. The two different copper positions are labeled. Hydrogen atoms adjacent to the in-chain oxygen atoms are omitted for clarity. Right: The corresponding diagram of a basic in-chain Heisenberg Hamiltonian with ferromagnetic J_1 and antiferromagnetic J_2 interactions (values are given in the text).

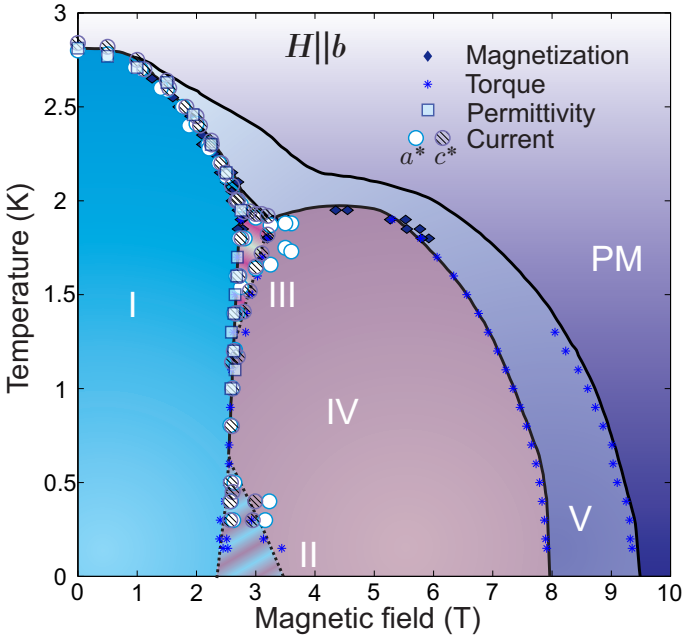

FIG. 2. Phase diagram of linarite for a field applied along the **b** direction. Following Ref. [16] the distinct thermodynamic phases are an elliptical spiral (I), a collinear Néel antiferromagnetic phase (IV), spin-density wave (V), and circular helix coexisting with collinear ordering (III). Phase II is supposed to be a metastable mixture of Phases I and IV. Solid lines are the phase boundaries according to Ref. [16], symbols are results of this work.

We have also carefully checked the magnetic phase diagram of our samples, and found it to be consistent with previous studies. As will be reported in detail elsewhere, to that end we used standard SQUID magnetometry (Quantum Design MPMS) and a home-built cantilever torque magnetometry setup. The corresponding experimental points, obtained for several samples, are shown in Fig. 2 (rhombi and crosses), in direct comparison with phase boundaries reported in Ref. [16] (lines).

For our dielectric experiments we have carefully selected a number of single crystals in which either the [100] or or [001] faces were well developed, and where the **b** direction could be clearly identified. A typical area of such faces was $1-2$ mm^2, with a typical transverse sample thickness of about 0.5 mm. The thus selected crystalline plates were sandwiched between external field electrodes. Correspondingly, the dielectric properties were probed either along the $\mathbf{a}^*$[21] or $\mathbf{c}^*$ directions. For each of these two cases, we used three principal measurement geometries: $\mathbf{H} \parallel \mathbf{b}$, $\mathbf{H} \parallel \mathbf{E}$ and $\mathbf{H} \parallel \mathbf{b} \times \mathbf{E}$. The dielectric permittivity was measured by an Andeen–Hagerling 2550A capacitance bridge using a 3-terminal scheme. Pyroelectric current measurements were performed with a Keithley 617A electrometer.

All experiments were carried out in a standard Dilution Refrigerator inset in the Quantum Design 9 T PPMS. This imposed some limitations for the types of pyro- or magnetoelectric current scans that could be performed: measuring current vs. T was feasible only in the range 1 K–4 K in the evaporative mode of DR operation. This configuration allowed us to achieve a good signal-to-noise ratio at temperature sweep rate of 0.5 K/min, while the difference between heating and cooling datasets still remained negligible. In the dilution cooling regime below 1 K the increase of thermal coupling times prevented a collection of meaningful current data in temperature sweeps. In contrast, measurements of current vs. H were possible at all temperatures down to approximately 0.2 K with an optimal sweeping rate of 0.01 T/sec.

III. RESULTS

A. Magnetic field along the b axis

Figure 3 shows a number of representative dielectric permittivity scans, measured with the electric field along the $\mathbf{a}^*$ direction. In contrast to the previous study by Yasui *et al.* [17], we do indeed find well-defined peaks in the dielectric permittivity occurring at the boundaries of Phase I. They are, unfortunately, too weak for a more quantitative investigation, but serve as markers of the phase transition and reveal the electrically active nature of the phase I. On the phase diagram of Fig. 2, their positions are plotted as squares. No further permittivity anomalies were detected in magnetic fields exceeding 3 T.

The phenomenology of current anomalies turned out to be much richer and easier to investigate. An important point is that we found the charge flow associated with the magnetic ordering to occur *spontaneously*, without any external voltage applied to the sample. Furthermore, moderate bias voltages (from +250 to -250 V) applied

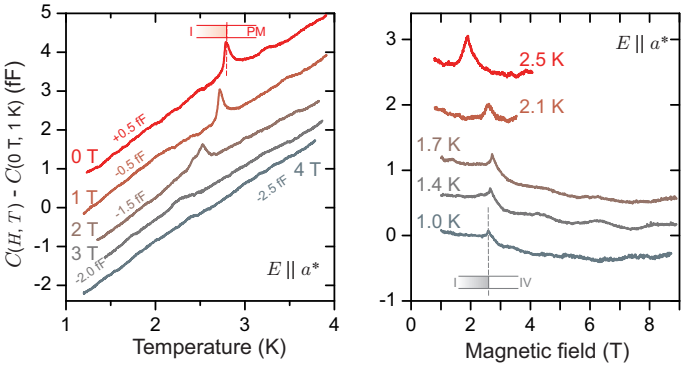

FIG. 3. Examples of measured $\mathbf{a}^*$-dielectric permittivity anomalies in linarite. The data are plotted as a difference between the measured capacitance and the reference value observed at $T = 1$ K, $H = 0$ T. On the left panel some constant offsets are additionally introduced for clarity. Phase boundaries according to Ref. [16] are marked for some of the curves.

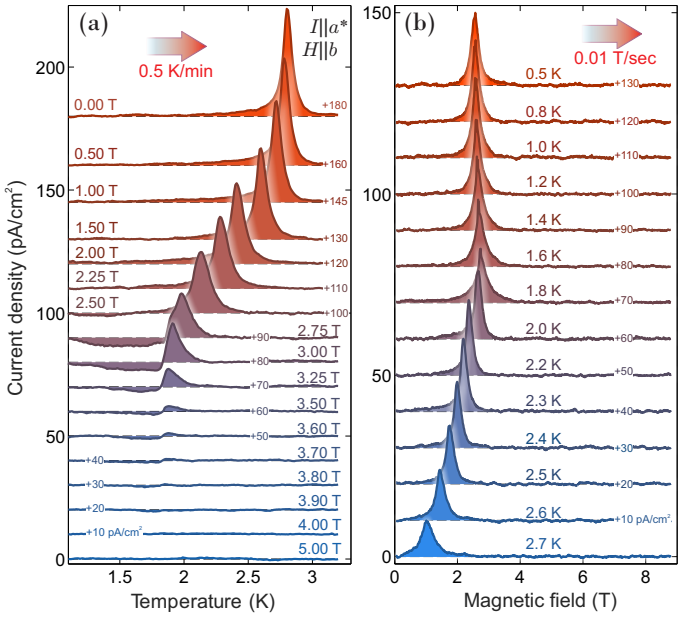

FIG. 4. Spontaneous current I_{a^*} through the sample (no bias voltage applied) in a magnetic field applied along the **b** direction. Panel (a) shows the pyroelectric current as a function of temperature during the warm-up, while panel (b) shows the magnetoelectric current in increasing magnetic field. The offsets are explicitly indicated. The zero level for each curve is shown as a dashed line.

to the sample during the cooldown process were only able to change the amount of the accumulated charge by ±30% without causing a sign reversal. This clearly indicates the existence of a preferred polarization (or spin chirality) direction, which is somewhat surprising for a centrosymmetric space group (as is $P2_1/m$ of linarite). Possible explanations of this finding will be discussed in Section IV B.

The pyroelectric current I_{a^*} measured in temperature

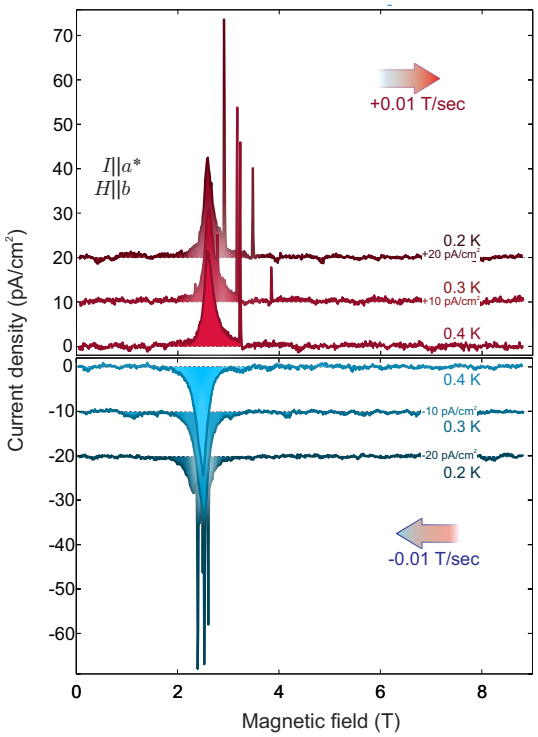

FIG. 5. Examples of up and down field scans of the I_{a^*} current below $T = 0.5$ K. The magnetic field is applied along the **b** direction. The difference between the scans with increasing and decreasing H, as well as the complex multi-peak response, is related to the metastability of the phase II.

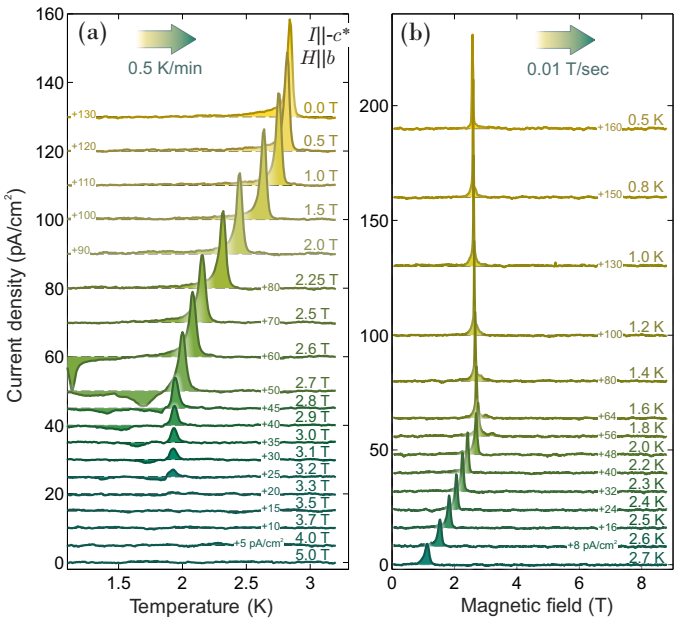

FIG. 6. The same, as in Fig. 4, but for the I_{c^*} component of current.

sweeps at several values of applied field is plotted in Fig. 4a. In zero magnetic field there is a prominent peak with maximum at $T_N \simeq 2.8$ K. This peak gradually broadens and shifts to lower temperatures with increasing field up to approximately 2.5 T. At this point, upon cooling, one enters the region labeled as III in Fig. 2. Here the pyroelectric current develops a more complex two-peak structure. First, charge goes into the sample during the cooldown into the Phase III, and then exits upon further cooling towards the Phase IV. Above 3.6 T no transition-related features in the pyroelectric current could be resolved at these temperatures. This shows the apparent non-electric character of Phases IV and V.

Isothermal magnetoelectric current measurements provide a complementary way of accessing the polarization. The field dependence of I_{a^*} is plotted in Fig. 4b for several temperatures. At the first glance there is just a single peak corresponding to the charge released on exiting Phase I. However, additionally there is a sharp current spike on top of the broader peak between 0.5 and 1.5 K. This marks a polarization discontinuity along what is a first-order phase transition line. The discontinuity becomes somewhat softened at lowest temperatures, when another region of phase coexistence is approached (phase II in the Fig. 2 phase diagram). As shown in Fig. 5, a rather complex behavior emerges below 0.5 K. On lowering the temperature the main peak becomes accompanied by multiple history-dependent sharp satellites. This directly reflects the metastable nature of Phase II [15]. No additional features could be found at higher magnetic field at any temperatures.

For the $\mathbf{c}^*$ component of current the situation is qualitatively similar. Examples of the I_{c^*} scans are shown in Fig. 6. The main difference is the weaker and much more abrupt character of the corresponding anomalies. The peaks in I_{c^*} are much narrower than in I_{a^*} at similar temperatures. This is especially pronounced below 1 K at the first order transition from Phase I to phase IV. At temperatures below 0.5 K a hysteretic multi-peak structure develops, similarly to that in I_{a^*} described above.

B. Magnetic field along the a* and a directions

Anomalies occurring in the current I_{a^*} as a function of temperature and magnetic field along the $\mathbf{a}^*$ direction are shown in Fig. 7. In small fields, the pyroelectric current behaves in a way similar to the $\mathbf{H} \parallel \mathbf{b}$ case. However, at higher fields a surprising two-peak structure is observed. The reversal of current direction corresponds to polarization reversal upon cooling. This behavior is also well pronounced in field scans (Fig. 7b) at lower temperatures. The charge release is slower than in the $\mathbf{H} \parallel \mathbf{b}$ case. This is why the amplitude of the I_{a^*} anomaly is seemingly reduced. Instead, the transition-related peak has a long tail stretching to low fields, reflecting the gradual evolution of the spiral structure towards the full saturation.

The current I_{c^*} in a magnetic field applied along $\mathbf{a}$ shows slightly different behavior (Fig. 8). We find only a single sharp peak at all fields and temperatures. In the low-T regime, it develops an extended tail, similarly to the I_{a^*} case discussed above.

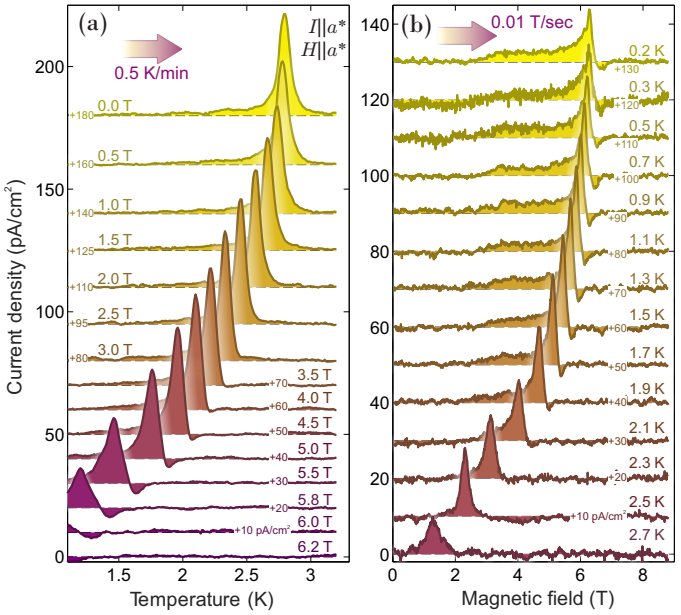

FIG. 7. The same, as in Fig. 4, but for the magnetic field $\mathbf{H} \parallel \mathbf{a}^*$.

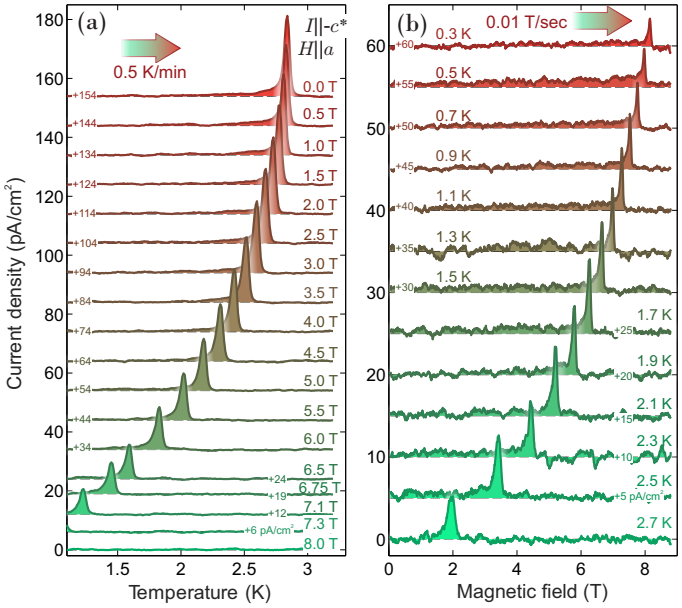

FIG. 8. The same, as in Fig. 6, but for the magnetic field $\mathbf{H} \parallel \mathbf{a}$.

C. Magnetic field along the c and c* directions

The cases of a magnetic field applied along the $\mathbf{c}$ and $\mathbf{c}^*$ directions appear to be the most trivial ones. There is

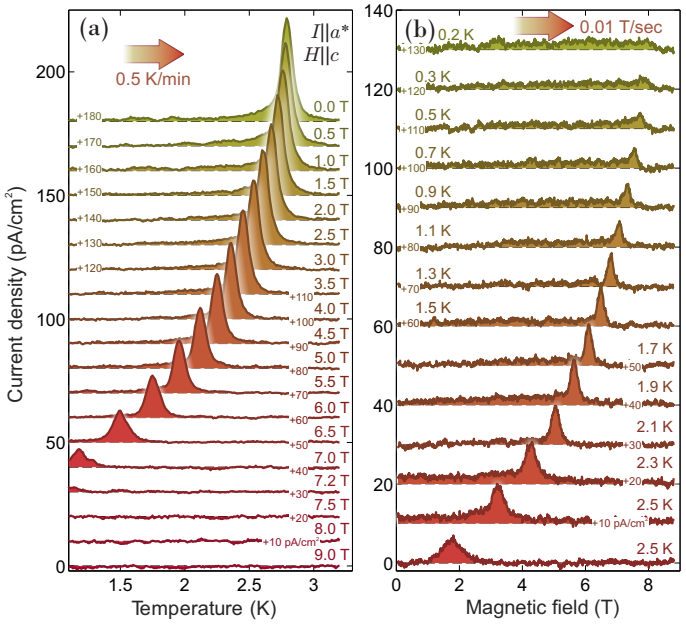

FIG. 9. The same, as in Fig. 4, but for the magnetic field $\mathbf{H} \parallel \mathbf{c}$.

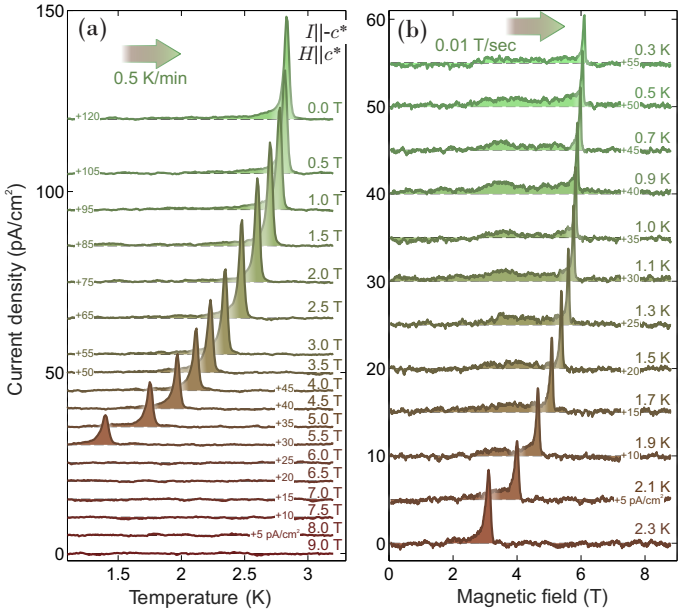

FIG. 10. The same, as in Fig. 6, but for the magnetic field $\mathbf{H} \parallel \mathbf{c}^*$.

always a single feature in the spontaneous current occurring at the phase boundary. A summary of I_{a^*} scans is present in Fig. 9. With lowering the temperature the peak becomes progressively less pronounced. Below 0.5 K, instead of peak, a small and almost constant current is detected within the ordered phase. This corresponds to an almost constant rate of charge release.

The c^*-component of electrical current measured in a magnetic field applied along the $\mathbf{c}^*$ direction is plotted

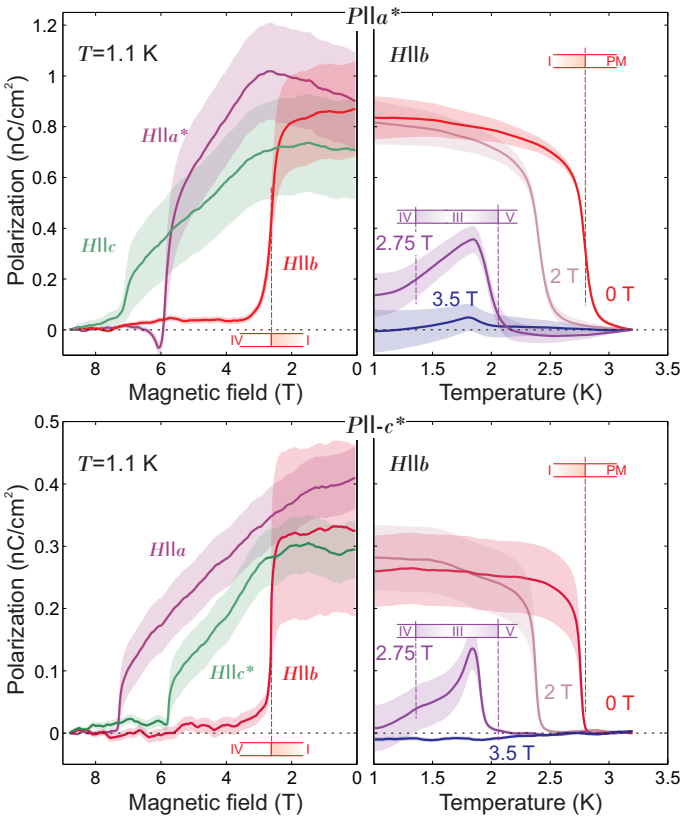

FIG. 11. Measured evolution of the polarization vector components as functions of magnetic field and temperature. The shaded areas show respective errors accumulating during the current integration procedure. Phase boundaries according to [16] are indicated for selected polarization curves.

in Fig. 10. The observed behavior is almost identical to that for $\mathbf{H} \parallel \mathbf{a}^*$.

IV. DISCUSSION

A. Polarization: a brief summary

In Figure 11 we compare representative field and temperature dependencies of different electric polarization components. These plots are deduced from T and H dependencies of I_{a^*} and I_{c^*} respectively, with the only assumption that the spontaneous polarization is totally absent at high fields and high temperatures. Along with the curves one can also see the associated uncertainty, estimated from the noise level during the measurement (those shaded areas also happen to be a fair estimate of the measurement reproducibility). The following phenomenology is evident from this data: in small magnetic fields the polarization emerges at the ordering temperature of Phase I, and then quickly saturates. One may argue that both components of $\mathbf{P}(T)$ are already saturated around 1 K. For a field applied along the $\mathbf{b}$ axis, the situation drastically changes around 2.5 T, where upon

cooling one consecutively enters first Phase III, and then Phase IV. Again, both components of $\mathbf{P}(T)$ rise around the corresponding transition temperature, but this is followed by a decrease upon further cooling. The magnitude of the polarization components is also noticeably reduced compared to those in Phase I. Finally, in higher fields, where only Phases IV and V are present, the electric polarization is absent.

The left panels of Fig. 11 show the magnetic field dependencies for the components of $\mathbf{P}(H)$ at $T = 1.1$ K. For $\mathbf{H} \parallel \mathbf{b}$ the polarization disappears in an abrupt way as the first-order phase transition from Phase I to Phase IV takes place. In contrast, for fields $\mathbf{H} \perp \mathbf{b}$ the decrease of $\mathbf{P}(H)$ is gradual, but with a clear onset point at the saturation field. We also would like to note the interesting behavior found in the P_{a^*} component of polarization in the magnetic field applied along $\mathbf{a}^*$ case. Here the P_{a^*} component changes its sign before fully disappearing in the paramagnetic phase. This feature will be discussed in more detail in Section IV E.

The actual values of saturation fields for different field directions deserve an additional comment. Confusingly, the saturation fields are similar for $\mathbf{H} \parallel \mathbf{a}^*, \mathbf{c}^*$ and $\mathbf{H} \parallel \mathbf{a}, \mathbf{c}$, but not for $\mathbf{H} \parallel \mathbf{a}^*, \mathbf{a}$ or $\mathbf{H} \parallel \mathbf{c}^*, \mathbf{c}$. This appears strange, given that the mismatch between the direct and reciprocal space vectors is only about 13°. The answer to the riddle is in the g tensor, completely mapped in Ref. [22]. Indeed, the principal axis of this tensor lie between the $\mathbf{a}$ and $\mathbf{c}$ directions in such a way that $g_c \simeq g_a$ and $g_{c^*} \simeq g_{a^*}$.

B. Polarization in Phase I

As it follows from Fig. 11, the polarization components are $P_{a^*} = 0.8 \pm 0.1$ and $P_{c^*} = 0.25 \pm 0.1$ nC/cm^2 in the low-temperature limit. This is in a rough agreement with the direction of vector $\mathbf{u}$ (see Fig. 12) that together with $\mathbf{b}$ defines the plane of the proposed spin spiral [16]. Surprisingly though, our measurements shows a clear and reproducible preference for a specific sign of the polarization. As the space group of the material is centrosymmetric, one would expect an approximately equal population of magnetic domains, differing by the sense of spiral rotation, and thus having opposite directions of $\mathbf{P}$. An external electric field would then alter the domain population. This kind of behavior was clearly demonstrated for $LiCuVO_4$, for example [9]. In contrast, in the present measurements on $PbCuSO_4(OH)_2$ the polarization direction, and thus the spin chirality, have a preferred direction even in the absence of biasing field. Furthermore, field-cooling in an applied electric field is unable to reverse the polarization. A potential explanation might be a strain in the sample, caused by the experimental environment at low temperatures. Improper ferroelectrics are known to be rather sensitive to elastic perturbations [23]. A somewhat more exciting but speculative explanation would be an unnoticed structural transition happening

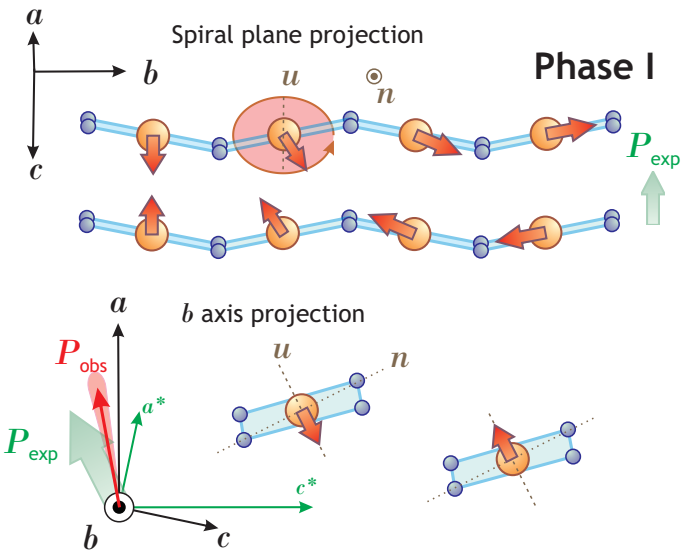

FIG. 12. The magnetic structure of Phase I according to Refs. [16, 18]. The direction of polarization dictated by the "inverse Dzyaloshinskii–Moriya mechanism" is indicated by a large green arrow. The observed polarization is shown by a red arrow, with the shaded area providing the experimental fan of uncertainty.

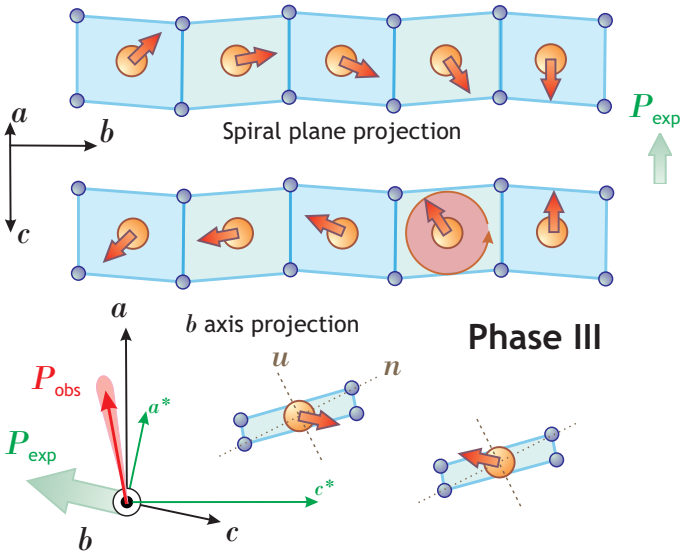

FIG. 13. Same as in Fig. 12, but for the field-induced Phase III. The observed direction of polarization is inconsistent with that deduced from the proposed magnetic structure.

at intermediate temperatures and leading to the loss of inversion symmetry. One example of a symmetry lowering transition, hardly noticeable structurally or thermodynamically, but having a profound effect on the magnetism has been recently discussed in Ref. [24].

C. Polarization in Phase III

Our measurements show that Phase I is not the only multiferroic phase of linarite. We also find clear signatures of ferroelectricity (mainly visible in temperature scans) in the Phase III. Neutron diffraction studies of Ref. [16] have suggested that phase to be of a mixed nature, with the intensity from incommensurate magnetic Bragg peaks gradually shifting to commensurate magnetic Bragg peaks (belonging to Phase IV). At the same time, even though the incommensurate propagation vector of Phase III is the same as in Phase I, $\mathbf{Q} = (0, -0.186, 0.5)$ r.l.u., the spin arrangement is claimed to be different. It was identified as circular helix with the rotation plane matching the $(\mathbf{b}, \mathbf{c})$ plane of the crystal. As the structure is still a spin spiral, the presence of electric polarization is not surprising. However, the observed direction of $\mathbf{P}$ is *inconsistent* with the proposed spin arrangement, as illustrated in Fig. 13. Indeed, in the "reverse Dzyaloshinskii–Moriya" mechanism necessarily $\mathbf{P} \propto [\mathbf{Q} \times \mathbf{n}]$. Therefore, a $(\mathbf{b}, \mathbf{c})$ planar spiral strictly requires the polarization to lie *within* the spiral plane. In contrast, experimentally the largest polarization component is observed along the direction $\mathbf{a}^*$, which is *normal* to this plane.

There are known cases of multiferroics with a relation between the spin structure and polarization vector that is much more complex than suggested by the straightforward "inverse Dzyaloshinskii–Moryia" mechanism [12, 13]. A very representative example is the triangular lattice antiferromagnet $RbFe(MoO_4)_2$ [25], where the electric polarization is exactly orthogonal to the helimagnetic planes. Cases like this require a more advanced symmetry-based treatment, as described in detail by Harris [26]. In linarite, however, the proposed model of the I–III phase transition does not seem to involve a significant change of magnetic state symmetry. Hence, it is not clear why it would invoke a completely different type of coupling between magnetism and polarization. This is especially strange given that the observed direction of $\mathbf{P}$ remains unchanged across the transition. Trying to make sense of this, we note that magnets with complex interactions often have very peculiar spin structures with multiple propagation vectors. One example is the spiral antiferromagnet $Ba_2CuGe_2O_7$, in which a very special antiferromagnetic cone phase described by simultaneous commensurate and incommensurate wave vectors was found [27]. The phenomenology of neutron diffraction observations in the $Ba_2CuGe_2O_7$ is remarkably similar to that in Phase III in linarite [16]. This analogy hints that Phase III in linarite may, in fact, also be a two-Q structure, rather than a mixed phase like Phase II. This idea is consistent with the stable character of electric anomalies in Phase III, and a history-dependent behavior found in Phase II.

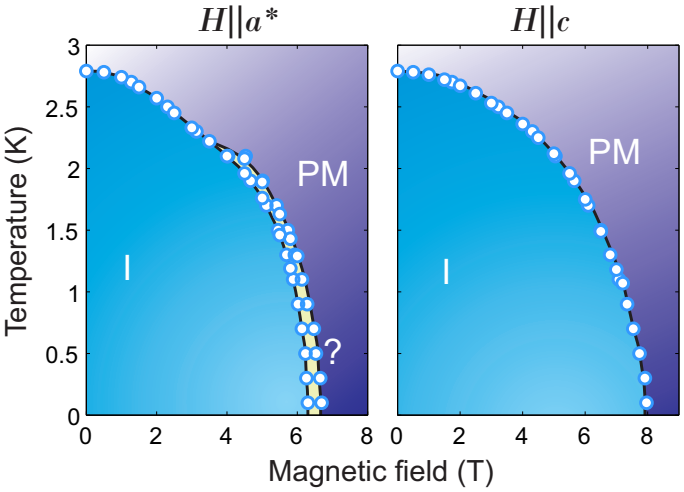

FIG. 14. Magnetic phase diagram of linarite deduced from electric current measurements for magnetic fields applied transverse to the $\mathbf{b}$ direction. Left panel: field along $\mathbf{a}^*$. The two dominant phases are Phase I and disordered paramagnetic state. In high fields there is an additional intervening region, although it is not clear if it represents a distinct thermodynamic phase. Right panel: field along the $\mathbf{c}$ direction. Symbols are experimental data, solid lines are guides for the eye.

D. Multiferroic metastability at low temperatures

As can be seen in Fig. 5, the situation with the isothermal magnetoelectric current becomes quite complicated as one touches the region denoted in the phase diagram (Fig. 2) as II. The evidence from the previous studies is that this metastable region corresponds to the coexistence of domains of Phases I and IV. This picture agrees well with our present observations. In this regime a well-defined anomaly corresponding to a first-order transition is replaced by a family of extremely sharp peaks that show a strong history dependence. In fact, each such spike manifests the loss of stability of a single Phase I domain (on increasing field) or Phase IV domain (on decreasing field). The observed spikes are just a differential multiferroic analogue of a familiar Barkhausen effect in ferromagnets.

E. Magnetic phase diagrams from electric measurements

The collected current data conveniently provides us with a way to reconstruct the magnetic phase diagram. The summary of our measurements is shown in Figs. 2 and 14. The phase diagram for the field applied in the $\mathbf{b}$ direction is clearly the most interesting one. Even though we find no electric activity in Phases IV and V, all the other ordered phases are proved to be multiferroic in nature.

We also find a peculiar behavior of polarization vec-

tor (polarization reversal) near saturation for a magnetic field applied in the $\mathbf{a}^*$ direction. According to Schäpers *et al.* [15], this phase diagram should contain a single elliptical spiral phase [28]. The abrupt reversal of polarization observed in our experiments is not necessarily indicative of a thermodynamic phase transition. It may just be a result of strong deformation of the spin structure by the magnetic field, as it becomes almost polarized. Neither can one fully exclude the spurious origin of this feature. The presence of misaligned grain in the sample may in principle result in this kind of behavior. On the other hand, the data for $\mathbf{H} \parallel \mathbf{b}$ and $\mathbf{H} \parallel \mathbf{c}$ taken on *the same sample* shows no phase boundary "splitting" in applied magnetic fields. Whether or not there is an additional phase in this geometry near saturation remains open.

The phase diagrams for magnetic fields applied in the $\mathbf{a}$, $\mathbf{c}$ and $\mathbf{c}^*$ directions undoubtedly contain just a single ordered phase with conventionally looking phase boundary. In Fig. 14 we show just one of such cases with $\mathbf{H} \parallel \mathbf{c}$.

V. SUMMARY

At least three of linarite's magnetic phases support spontaneous electric polarization: i) The principal spin spiral state (Phase I) appears to be a classic "reverse Dzyaloshinskii–Moriya" improper ferroelectric. The observed direction of polarization is fully consistent with the magnetic structure proposed in Refs. [16, 18]. ii) Also in agreement with Ref. [15], the region II found between the spiral Phase I and the collinear Phase IV is actually a phase-separation regime, showing a typical history dependent behavior of polarization. iii) The polarization observed in Phase III is *not* consistent with the phase-separated magnetic state proposed in Ref. [16]. Rather, it appears to be a stable thermodynamic phase and may be a complex multi-Q spin structure. iv) A new region of polarization reversal, which may or may not be a distinct thermodynamic phase, is identified close to saturation for a magnetic field applied along the $\mathbf{a}^*$ direction.

ACKNOWLEDGMENTS

This work was supported by the Swiss National Science Foundation, Division 2. We also thank Dr. S. Gvasaliya (ETH Zürich) for support with experiments.

[1] D. I. Khomskii, "Multiferroics: Different ways to combine magnetism and ferroelectricity," J. Magn. Magn. Mater. **306**, 1 (2006).
[2] S.-W. Cheong and M. Mostovoy, "Multiferroics: a magnetic twist for ferroelectricity," Nat. Mater. **6**, 13 (2007).
[3] Y. Tokura, S. Seki, and N. Nagaosa, "Multiferroics of spin origin," Rep. Prog. Phys. **77**, 076501 (2014).
[4] T. Goto, T. Kimura, G. Lawes, A. P. Ramirez, and Y. Tokura, "Ferroelectricity and Giant Magnetocapacitance in Perovskite Rare-Earth Manganites," Phys. Rev. Lett. **92**, 257201 (2004).
[5] F. Kagawa, M. Mochizuki, Y. Onose, H. Murakawa, Y. Kaneko, N. Furukawa, and Y. Tokura, "Dynamics of Multiferroic Domain Wall in Spin-Cycloidal Ferroelectric $DyMnO_3$," Phys. Rev. Lett. **102**, 057604 (2009).
[6] F. Schrettle, S. Krohns, P. Lunkenheimer, A. Loidl, E. Wulf, T. Yankova, and A. Zheludev, "Magnetic-field induced multiferroicity in a quantum critical frustrated spin liquid," Phys. Rev. B **87**, 121105 (2013).
[7] K. Yu Povarov, A. Reichert, E. Wulf, and A. Zheludev, "Giant dielectric nonlinearities at a magnetic Bose-Einstein condensation," Phys. Rev. B **92**, 140410 (2015).
[8] S. Park, Y. J. Choi, C. L. Zhang, and S-W. Cheong, "Ferroelectricity in an $s = 1/2$ chain cuprate," Phys. Rev. Lett. **98**, 057601 (2007).
[9] M. Mourigal, M. Enderle, R. K. Kremer, J. M. Law, and B. Fåk, "Ferroelectricity from spin supercurrents in $LiCuVO_4$," Phys. Rev. B **83**, 100409 (2011).
[10] S. Seki, Y. Yamasaki, M. Soda, M. Matsuura, K. Hirota, and Y. Tokura, "Correlation between Spin Helicity and an Electric Polarization Vector in Quantum-Spin Chain Magnet $LiCu_2O_2$," Phys. Rev. Lett. **100**, 127201 (2008).
[11] S. Furukawa, M. Sato, and S. Onoda, "Chiral Order and Electromagnetic Dynamics in One-Dimensional Multiferroic Cuprates," Phys. Rev. Lett. **105**, 257205 (2010).
[12] H. Katsura, N. Nagaosa, and A. V. Balatsky, "Spin current and magnetoelectric effect in noncollinear magnets," Phys. Rev. Lett. **95**, 057205 (2005).
[13] M. Mostovoy, "Ferroelectricity in spiral magnets," Phys. Rev. Lett. **96**, 067601 (2006).
[14] M. Baran, A. Jedrzejczak, H. Szymczak, V. Maltsev, G. Kamieniarz, G. Szukowski, C. Loison, A. Ormeci, S.-L. Drechsler, and H. Rosner, "Quasi-one-dimensional $S = 1/2$ magnet $Pb[Cu(SO_4(OH)_2]$: frustration due to competing in-chain exchange," Phys. Status Solidi C **3**, 220 (2006).
[15] M. Schäpers, A. U. B. Wolter, S.-L. Drechsler, S. Nishimoto, K.-H. Müller, M. Abdel-Hafiez, W. Schottenhamel, B. Büchner, J. Richter, B. Ouladdiaf, M. Uhlarz, R. Beyer, Y. Skourski, J. Wosnitza, K. C. Rule, H. Ryll, B. Klemke, K. Kiefer, M. Reehuis, B. Willenberg, and S. Süllow, "Thermodynamic properties of the anisotropic frustrated spin-chain compound linarite $PbCuSO_4(OH)_2$," Phys. Rev. B **88**, 184410 (2013).
[16] B. Willenberg, M. Schäpers, A. U. B. Wolter, S.-L. Drechsler, M. Reehuis, J.-U. Hoffmann, B. Büchner, A. J. Studer, K. C. Rule, B. Ouladdiaf, S. Süllow, and S. Nishimoto, "Complex Field-Induced States in Linarite $PbCuSO_4(OH)_2$ with a Variety of High-Order Exotic Spin-Density Wave States," Phys. Rev. Lett. **116**, 047202 (2016).

[17] Y. Yasui, M. Sato, and I. Terasaki, "Multiferroic Behavior in the Quasi-One-Dimensional Frustrated Spin-1/2 System $PbCuSO_4(OH)_2$ with CuO_2 Ribbon Chains," J. Phys. Soc. Jap. **80**, 033707 (2011).

[18] B. Willenberg, M. Schäpers, K. C. Rule, S. Süllow, M. Reehuis, H. Ryll, B. Klemke, K. Kiefer, W. Schottenhamel, B. Büchner, B. Ouladdiaf, M. Uhlarz, R. Beyer, J. Wosnitza, and A. U. B. Wolter, "Magnetic Frustration in a Quantum Spin Chain: The Case of Linarite $PbCuSO_4(OH)_2$," Phys. Rev. Lett. **108**, 117202 (2012).

[19] A. U. B. Wolter, F. Lipps, M. Schäpers, S.-L. Drechsler, S. Nishimoto, R. Vogel, V. Kataev, B. Büchner, H. Rosner, M. Schmitt, M. Uhlarz, Y. Skourski, J. Wosnitza, S. Süllow, and K. C. Rule, "Magnetic properties and exchange integrals of the frustrated chain cuprate linarite $PbCuSO_4(OH)_2$," Phys. Rev. B **85**, 014407 (2012).

[20] H. G. Bachmann and J. Zemann, "Die Kristallstruktur von Linarit PbCuSO4(OH)2," Acta Crystallographica **14**, 747 (1961).

[21] As in the standard reciprocal lattice notation.

[22] M. Schäpers, H. Rosner, S.-L. Drechsler, S. Süllow, R. Vogel, B. Büchner, and A. U. B. Wolter, "Magnetic and electronic structure of the frustrated spin-chain compound linarite $PbCuSO_4(OH)_2$," Phys. Rev. B **90**, 224417 (2014).

[23] V. Dvořák, "Improper ferroelectrics," Ferroelectrics **7**, 1 (1974).

[24] M. Hälg, D. Hüvonen, T. Guidi, D. L. Quintero-Castro, M. Boehm, L. P. Regnault, M. Hagiwara, and A. Zheludev, "Finite-temperature scaling of spin correlations in an experimental realization of the one-dimensional Ising quantum critical point," Phys. Rev. B **92**, 014412 (2015).

[25] M. Kenzelmann, G. Lawes, A. B. Harris, G. Gasparovic, C. Broholm, A. P. Ramirez, G. A. Jorge, M. Jaime, S. Park, Q. Huang, A. Ya. Shapiro, and L. A. Demianets, "Direct transition from a disordered to a multiferroic phase on a triangular lattice," Phys. Rev. Lett. **98**, 267205 (2007).

[26] A. B. Harris, "Landau analysis of the symmetry of the magnetic structure and magnetoelectric interaction in multiferroics," Phys. Rev. B **76**, 054447 (2007).

[27] S. Mühlbauer, S. N. Gvasaliya, E. Pomjakushina, and A. Zheludev, "Double-k phase of the Dzyaloshinskii-Moriya helimagnet $Ba_2CuGe_2O_7$," Phys. Rev. B **84**, 180406 (2011).

[28] Nonetheless, we note that the last non-featureless specific heat curve in the corresponding panel of Fig. 9 in Ref. [15] may give some room for speculation.